Dynamics of wind and the dusty environments in the accreting T Tauri stars RY Tauri and SU Aurigae

P Petrov, K Grankin, J Gameiro, S Artemenko, E Babina, R de Albuquerque, A Djupvik, G Gahm, V Shenavrin, T Irsmambetova, et al.

Monthly Notices
of the
ROYAL ASTRONOMICAL SOCIETY

MNRAS **483,** 132–146 (2019) doi:10.1093/mnras/sty3066

Dynamics of wind and the dusty environments in the accreting T Tauri stars RY Tauri and SU Aurigae

P. P. Petrov [1]★ K. N. Grankin,[1] J. F. Gameiro [2,3]★ S. A. Artemenko,[1] E. V. Babina,[1] R. M. G. de Albuquerque,[2,3,4] A. A. Djupvik,[5] G. F. Gahm,[6] V. I. Shenavrin,[7] T. R. Irsmambetova,[7] M. Fernandez,[8] D. E. Mkrtichian[9] and S. Yu. Gorda[10]

[1] *Crimean Astrophysical Observatory of Russian Academy of Sciences, p/o Nauchny, 298409, Republic of Crimea*
[2] *Instituto de Astrofísica e Ciências do Espaço, Universidade do Porto, CAUP, Rua das Estrelas, PT4150-762 Porto, Portugal*
[3] *Departamento de Física e Astronomia, Faculdade de Ciências, Universidade do Porto, Rua do Campo Alegre 687, PT4169-007 Porto, Portugal*
[4] *Laboratoire Univers et Théories, Observatoire de Paris, UMR 8102 du CNRS, Université Paris Diderot, F-92190 Meudon, France*
[5] *Nordic Optical Telescope, Rambla José Ana Fernández Pérez, 7, 38711 Breña Baja, Spain*
[6] *Department of Astronomy, AlbaNova University Center, Stockholm University, Sweden*
[7] *Sternberg Astronomical Institute, M. V. Lomonosov Moscow State University, Moscow, Russia*
[8] *Institute of Astrophysics of Andalusia-CSIC, Glorieta de la Astronomía, 3, 18008 Granada, Spain*
[9] *National Astronomical Research Institue of Thailand, 260 Moo 4, T. Donkaew, A. Maerim, Chiangmai, 50180 Thailand*
[10] *Ural Federal University, 51, Lenin av., Ekaterinburg 620000, Russia*

Accepted 2018 November 7. Received 2018 November 7; in original form 2018 June 4

ABSTRACT

Classical T Tauri stars with ages of less than 10 Myr possess accretion discs. Magnetohydrodynamic processes at the boundary between the disc and the stellar magnetosphere control the accretion and ejections gas flows. We carried out a long series of simultaneous spectroscopic and photometric observations of the classical T Tauri stars, RY Tauri and SU Aurigae, with the aim to quantify the accretion and outflow dynamics at time-scales from days to years. It is shown that dust in the disc wind is the main source of photometric variability of these stars. In RY Tau, we observed a new effect: during events of enhanced outflow, the circumstellar extinction becomes lower. The characteristic time of changes in outflow velocity and stellar brightness indicates that the obscuring dust is near the star. The outflow activity in both stars is changing on a time-scale of years. Periods of quiescence in the variability of the Hα profile were observed during the 2015–2016 period in RY Tau and during the 2016–2017 period in SU Aur. We interpret these findings in the framework of the magnetospheric accretion model, and we discuss how the global stellar magnetic field can influence the long-term variations of the outflow activity.

Key words: line: profiles – stars: individual: RY Tau – stars: individual: SU Aur – stars: variables: T Tauri, Herbig Ae/Be – stars: winds, outflows.

1 INTRODUCTION

Young stars possess accretion discs at the beginning of their evolution. For solar-mass stars, the lifetimes of these discs are a few million years. Eventually, the disc dissipates and the mass accretion ceases. Classical T Tauri stars (cTTSs) are young low-mass stars ($M < 2$–$3\ M_\odot$) with accretion discs. Their characteristic emission-line spectrum, irregular light variability and non-stationary outflows are consequences of the interaction of the accreting gas with the stellar magnetic field. When accretion ceases, the outflows disappear and the emission-line spectra become weak. These are the weak-line T Tauri stars (wTTSs). This phase is much longer, 10–100 Myr, until the star eventually reaches the main sequence.

The current view of cTTSs and their environments is based on the magnetospheric accretion model, initially designed for neutron stars (Ghosh & Lamb 1979) and later applied for cTTSs (Camenzind 1990; Koenigl 1991). According to the models, the accretion disc of a cTTS is truncated by a stellar magnetic field at a distance of a few stellar radii. The magnetic field penetrates the inner part of the disc and thus the gas of the disc can flow down to the stellar surface along the field lines. A shock is formed at the base of the accretion channel. X-ray and ultraviolet (UV) radiation of the accretion shock ionize the infalling gas, thus giving rise to the characteristic emission-line spectrum of a cTTS. The mass accretion rates in cTTSs are in the range of 10^{-10} to $10^{-7}\ M_\odot\ yr^{-1}$. The radii of the inner accretion disc in cTTSs, measured by near-infrared (NIR) interferometry,

★ E-mail: petrov@craocrimea.ru (PPP); jgameiro@astro.up.pt (JFG)

are typically within 0.1–0.3 au (Millan-Gabet et al. 2007). The observed properties and models of cTTSs can be found in reviews by, for example, Petrov (2003), Bouvier et al. (2007) and Hartmann, Herczeg & Calvet (2016).

Besides the accretion flows, cTTSs are also characterized by powerful outflows. Large-scale ordered magnetic fields are thought to play a key role in forming these gas flows. Different types of winds have been considered, including a stellar wind flowing along the open magnetic field lines in the polar regions of the star (Cranmer 2009), and a disc wind, starting from the extended surface of the accretion disc and accelerated by the magnetic centrifuge of the rotating disc (Blandford & Payne 1982; Pudritz & Norman 1986; Matt & Pudritz 2005). Other possible types of winds originate from the inner region of the disc, at the boundary between the disc and the magnetosphere, either as a so-called X-wind (Shu et al. 1994) or a conical wind (Romanova et al. 2009). The region where the magnetic flux connects the disc with the star is very unstable, where magnetospheric ejections of plasma can take place (Goodson, Winglee & Böhm 1997; Zanni & Ferreira 2013). Magnetohydrodynamic (MHD) simulations of the accretion and outflow processes in cTTSs have been performed by several groups; see the reviews by Bouvier et al. (2007) and Romanova & Owocki (2015), and references therein. The gas flows can be traced by analysis of emission-line profiles in the spectra of cTTSs. Specific profiles of hydrogen and helium lines were calculated for different wind models (e.g., Kurosawa, Romanova & Harries 2011; Grinin, Tambovtseva & Weigelt 2012). The disc wind also contributes to the irregular light variability of cTTSs. Beyond the dust sublimation radius, the disc wind is dusty, which causes circumstellar extinction of cTTSs.

The processes of accretion and accretion-driven winds are non-stationary. The dynamics of the gas flows depends on the conditions at the boundary between the disc and stellar magnetosphere. The stellar magnetosphere might not be axisymmetric, which causes rotational modulation of the observed flows. Rotational modulations in emission lines have been observed in some cTTSs, such as RW Aur A (Petrov 2003), and have also been simulated in MHD models (e.g. Romanova et al. 2007).

Long-term variations in the outflow activity can be controlled by the variable mass accretion rate and/or the gradual change in the global stellar magnetic field. Variations in the magnetic fields of cTTSs have been reported by Donati et al. (2011, 2012).

In this paper, we present the results of our spectroscopic monitoring of two cTTSs, SU Aur and RY Tau, over several years. Besides long-term changes in the wind activity, we were interested to know whether short-term wind dynamics is reflected in the irregular variations of the circumstellar extinction. For this reason, the spectroscopy was supported by simultaneous photometry of the stars. Preliminary results of the first two years of our monitoring of RY Tau have previously been published in Babina, Artemenko & Petrov (2016).

The paper is organized as follows. In Section 2, we start with a review of the basic data for SU Aur and RY Tau. We give a description of our observations in Section 3. The results obtained are given in Section 4 and are discussed in Section 5. Finally, the conclusions are listed in Section 6.

2 BASIC DATA FOR SU AUR AND RY TAU

In this section, we compare the observed characteristics of RY Tau and SU Aur in order to outline their similarities and differences. Both stars belong to intermediate-mass cTTSs. They are located in the Taurus–Auriga star-forming region at a distance of about 140 pc (Elias 1978; Loinard et al. 2007). The basic parameters of the stars according to Calvet et al. (2004) are $T_{\rm eff} = 5945 \pm 142.5$ K for both stars and stellar luminosities L are 9.6 ± 1.5 $L_\odot$ in RY Tau and 7.8 ± 1.3 $L_\odot$ in SU Aur.

The parallaxes measured by *Gaia*[1] (Gaia Collaboration et al. 2016a, 2016b) give the following distances: 142.4 ± 12 pc for SU Aur and 176.6 ± 27 pc for RY Tau . That is, the distance to RY Tau could be larger than is usually assumed. However, we should take into account the most accurate measurements of parallaxes of several TTSs in the Taurus complex obtained in the multi-epoch Very Long Baseline Array (VLBA) observations by Loinard et al. (2007). They found a mean distance to the star-forming region of about 140 pc with a depth of around 20 pc. Hence, the upper limit of the distances measured by the VLBA (150 pc) coincides with the lower limit of the distance to RY Tau (149.6 pc) obtained by *Gaia*. Therefore, we adopt a distance to RY Tau of 150 ± 10 pc.

2.1 Light variability

Both objects have long photometric records. RY Tau has shown irregular variability within $V = 9.5-11.5$, with noticeable brightening during the periods 1983–1984 and 1996–1997 (Herbst & Stine 1984; Herbst et al. 1994; Zajtseva et al. 1996). The most extended series of photometric observations of RY Tau from 1965 to 2000 was analysed by Zajtseva (2010). Quasi-periodic variations of brightness, probably associated with eclipses by dust clouds in the circumstellar disc, were revealed. No periodicity related to the rotation of the star itself was detected.

SU Aur is an irregular variable, most of time at $V = 9.0-9.5$ with random drops down to $V = 10-11$ (Herbst & Shevchenko 1999; DeWarf et al. 2003). Possible periods of 1.55 and 2.73 d were reported by Herbst et al. (1987), but not confirmed later (Herbst & Koret 1988). Bouvier, Bertout & Bouchet (1988) and Bouvier et al. (1993) reported a possible period of 2.78 d, which is close to the rotational period derived from spectral-line variations (see below). Photometry from the *Microvariablity and Oscillations of Stars* (*MOST*) mission (Cody et al. 2013) showed small amplitude ($\sim$0.1 mag) brightness oscillations with a period of $\sim$2.7 d over 20 d of observations.

2.2 Emission-line spectra

The emission-line spectra of RY Tau and SU Aur are not as strong as in late-type cTTSs, because of the luminous background of the G-type photosphere. In the optical spectrum of SU Aur, only Hα is in the emission. In RY Tau, the emission spectrum includes Hα, Hβ, the Na I doublet, He I 5876 Å, Ca II doublet and the NIR Ca II triplet (e.g. Hamann & Persson 1992; Alencar & Basri 2000). Forbidden emission lines of [O I], [N II], [S II] and [Fe II] were observed in the spectrum of RY Tau (Cabrit et al. 1990; Akitaya et al. 2009). No forbidden lines have been reported for SU Aur.

The photospheric spectrum of a cTTS is often veiled by additional radiation from hot surface areas at the base of accretion columns. The effect is stronger in a late-type cTTS where the brightness contrast of the hot area is larger. The veiling of the photospheric spectrum of RY Tau in the visual range is very low or absent (Basri, Martin & Bertout 1991; Hartigan, Edwards & Ghandour 1995; Petrov et al. 1999; Chou et al. 2013). No veiling in the visible photospheric spectrum of SU Aur has been reported. Excess continuous radiation

[1] See http://gaia.ari.uni-heidelberg.de/singlesource.html.

is present in the far-UV spectrum of both stars, larger in RY Tau than in SU Aur. The mass accretion rates, estimated from the accretion luminosities in UV, are 6.4–9.1 ± 4.9 for RY Tau and 0.5–0.6 ± 0.4 for SU Aur, in units of 10^{-8} $M_\odot$ yr^{-1} (Calvet et al. 2004).

Near-UV and far-UV spectra of TTSs, including RY Tau and SU Aur, were analysed by Ardila et al. (2002), Gomez de Castro & Verdugo (2007) and Gomez de Castro & Marcos-Arenal (2012). A catalogue of selected atomic and molecular line fluxes, observed in the far-infrared, is presented in Alonso-Martinez et al. (2017).

2.3 Rotation and X-rays

Both stars are rapid rotators. In SU Aur, $v \sin i$ is within 60–66 km s^{-1}(Nguyen et al. 2012; Johns-Krull 1996; Petrov et al. 1996). In RY Tau, $v \sin i \sim 50$ km s^{-1}(Petrov et al. 1999). The rotation period of SU Aur is within 2.7–3.0 d, as determined from periodical modulations of the blueshifted and redshifted absorption components in the Balmer line profiles (Giampapa et al. 1993; Johns & Basri 1995; Petrov et al. 1996) and the strength of He I emission lines (Unruh et al. 2004). In RY Tau, no rotation period was detected, from either the extended photometric series or the emission-line variations. Both RY Tau and SU Aur are X-ray sources. RY Tau is a strong, flaring X-ray source, indicating radiation from a hot plasma at $T \sim 50$ MK. The flaring component is undoubtedly of magnetic origin (Skinner, Audard & Gudel 2016). The quiescent X-ray emission from SU Aur is dominated by a 20–40 MK plasma, while an extremely high-temperature plasma component (at least 60 MK) was observed in a flare (Smith et al. 2005).

2.4 Discs and jets

Both stars possess accretion discs, as indicated by their spectral energy distribution (SED) and interferometry in the IR. The SED of RY Tau and SU Aur from *Spitzer* mid-IR observations (Furlan et al. 2011) represents radiation of warm layers from an inner disc within 10 au.

A number of accretion disc models of RY Tau and SU Aur have been presented to reproduce the IR observations (e.g. Muzerolle et al. 2003; Akeson et al. 2005; Schegerer et al. 2008; Isella, Carpenter & Sargent 2010; Guilloteau et al. 2011). The inner disc radius in different models drops to within 0.3–0.5 au, and inclinations of the disc axis to the line of sight appear within 55–75°.

Imaging polarimetry of SU Aur has shown that the accretion disc extends out to 500 au with an inclination of ∼50° (Jeffers et al. 2014); the disc morphology with tidal tails was reconstructed by De Leon et al. (2015). Imaging polarimetry of RY Tau (Takami et al. 2013) showed that the scattered light in the NIR is associated with an optically thin and geometrically thick layer above the disc surface. The changes in the linear polarization across the Hα line in RY Tau and SU Aur are consistent with the presence of a compact source of line emission that is scattered off a rotating inner accretion disc (Vink et al. 2005).

Extended bipolar jets of RY Tau, with young dynamical ages of the inner knots, were detected in Hα light (St-Onge & Bastien 2008) and mapped in [O I] 6300 Å (Agra-Amboage et al. 2009). Spatially resolved C IV emission from the blueshifted jet of RY Tau has been detected by Skinner et al. (2018).

In summary, RY Tau and SU Aur are similar with regard to their stellar parameters, but with different accretion rates and circumstellar environments. The high inclination of both stars implies that the line of sight intersects the disc winds. This provides an opportunity to search for dynamics of the circumstellar gas flows through variability in spectral-line profiles.

2.5 Spectral time series

A typical characteristic of the gas flow in cTTSs is its non-stability on time-scales of 1 d or longer. In some cases, spectral monitoring can reveal modulation of a line profile with a period of the stellar rotation, which might be a result of axial asymmetry of the gas flows.

Several extended time series of high-resolution spectroscopic observations have been obtained for SU Aur (Giampapa et al. 1993; Johns & Basri 1995; Petrov et al. 1996; Oliveira et al. 2000; Unruh et al. 2004). The Balmer line profiles show the largest variability in the blueshifted and redshifted depressions of the broad emission profiles, formed in the outflow (wind) and inflow (accretion) gas streams. Variations in the blue wing of Hα and Hβ revealed a rotational period about 3.0 d (Giampapa et al. 1993; Johns & Basri 1995; Petrov et al. 1996). A shorter period of 2.6–2.8 d was found in variations of the He I D3 line (Unruh, Solanki & Fligge 2000; Unruh et al. 2004). Time series involving Paβ spectroscopy of SU Aur over three consecutive nights showed relatively strong variability in the red wing within a radial velocity range of 100–420 km s^{-1}, and less variability in the blue wing. A model with an inclined dipole magnetosphere reproduced the observed line variability (Kurosawa, Harries & Symington 2005). Sometimes, a strong depression of the blue wing of Hα appeared, indicating enhanced sporadic mass ejections (Petrov et al. 1996).

The time variability of the emission lines in RY Tau has been studied by Zajtseva et al. (1985), Petrov (1990), Johns & Basri (1995), Smith et al. (1999), Mendigutía et al. (2011) and Chou et al. (2013). The broad emission profile of the Hα line is cut by a deep blueshifted depression. Both the blue and red peaks of the line are variable on a time-scale of a few days. Balmer Hα line monitoring of RY Tau over 37 almost fully contiguous nights (Johns & Basri 1995) did not reveal any periodicity similar to SU Aur. Although both RY Tau and SU Aur are fast rotators with similar stellar parameters, the axial rotation of RY Tau is not reflected as variability in the Balmer line profiles. Ismailov, Adigezalzade & Bahaddinova (2015) reported a possible period of 23 d in variability of the Mg II 2800 Å emission-line intensity in the *International Ultraviolet Explorer* (*IUE*) spectra of RY Tau. This is close to the periods found from photometric series (Bouvier et al. 1993; Gahm et al. 1993a). This long period is certainly not related to the stellar rotation.

3 OBSERVATIONS

Our spectral and photometric observations were carried out during five periods over 2013–2018. We started with observations of RY Tau at the Crimean Astrophysical Observatory (CrAO) in 2013–2014 and 2014–2015. Then, a multisite monitoring of RY Tau and SU Aur was arranged during 2015–2016. Later, we proceeded with observations of RY Tau and SU Aur, mostly at CrAO. In all periods, the photometry of our targets was performed at three telescopes, located in Crimea.

3.1 Spectroscopy

The following five instruments were used to obtain series of spectral observations of RY Tau and SU Aur:

(i) the 2.6-m Shajn reflector of the CrAO with the echelle spectrograph (spectral resolution $R = 27\,000$ with an entrance slit of 2 arcsec).

(ii) the 2.5-m Nordic Optical Telescope (NOT) with the ALFOSC grism spectrograph, grism set #17 (registered spectral region 6330–6870 Å and $R = 10\,000$ with an entrance slit of 0.5 arcsec).

(iii) the 2.2-m telescope at Centro Astronómico Hispano-Alemán (CAHA) with the CAFE echelle spectrograph ($R = 58\,000$ with an entrance slit of 1.2 arcsec).

(iv) the 2.4-m Thai National Telescope (TNT) at the Thai National Observatory (TNO) with the medium resolution spectrograph (MRES; $R = 19\,000$ with an entrance fibre of 2 arcsec).

(v) the 1.2-m telescope of the Kourovka Astronomical Observatory of the Ural Federal University (UrFU), with the fibre-fed echelle spectrograph ($R = 15\,000$ with an entrance fibre of 5 arcsec; Panchuk, Yushkin & Yakopov 2011).

Further details on the spectrographs can be found on the websites of the observatories. All spectra were reduced and wavelength calibrated using standard procedures and IRAF tools.[2] In the echelle spectra, we utilized only those spectral orders that cover regions of the Hα and Na D lines. The signal-to-noise ratio per resolution element at the continuum level in all the spectra was over 100. The total number of nights of spectral observations was 127 for RY Tau and 96 for SU Aur. A log of spectral observations is given in Tables A1 and A2.

3.2 Photometry

Optical photometry of RY Tau and SU Aur in the Johnson *BVRI* photometric system was carried out with two instruments: the 1.25-m telescope (AZT-11) of the CrAO and the 0.6-m telescope (Zeiss-600) at the Crimean Astronomical Station (CAS) of Moscow State University. At the 1.25-m telescope, a photometer with a FLI PL23042 CCD camera was used for routine differential photometry, while in cases of a perfectly clear sky a photocounting photometer was used for absolute photometry. The standard error is about 0.02 mag in all bands. At the 0.6-m telescope, a photometer with CCD cameras Apogee Aspen and PL4022 was used.

NIR photometry was carried out at the 1.25-m telescope of the CAS. An InSb photometer with a standard *JHKLM* system was used. The technical parameters of the photometer, the methods of observations and the calculations of magnitudes have been described in detail by Shenavrin, Taranova & Nadzhip (2011). Stars BS1203 and BS1791 were used as standards for RY Tau and SU Aur, respectively. The *JKL* magnitudes of the standards were taken from the catalogue of Johnson et al. (1966), and the *HM* magnitudes were calculated from relations given in Koornneef (1983). The standard error of the measured magnitudes is about 0.02 in the *JHKL* bands, and about 0.05 in the *M* band. In addition, we used also photometric data from the American Association of Variable Star Observers (AAVSO; Kafka 2017).

The results of the photometric observations in the *V* band are presented in the form of light curves in Figs 1 and 2, where moments of spectral observations are marked with vertical bars. The AAVSO data are added to the figure to make the light curves more dense. The *V* magnitudes for the dates of spectral observations are also

[2]IRAF is distributed by the National Optical Astronomy Observatory, which is operated by the Association of Universities for Research in Astronomy (AURA) under cooperative agreement with the National Science Foundation.

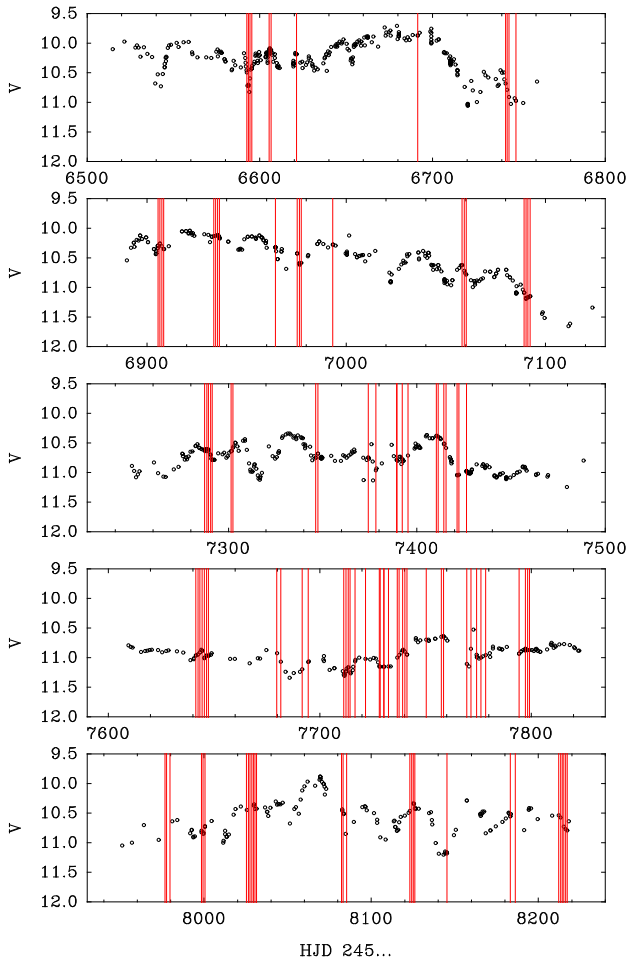

Figure 1. Light curves of RY Tau in five periods, from 2013–2014 (upper panel) to 2017–2018 (lower panel). Vertical lines mark the moments of spectral observations.

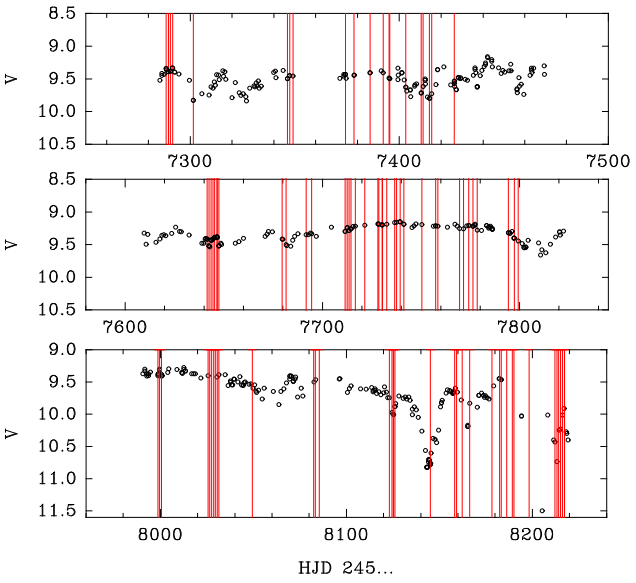

Figure 2. Light curves of SU Aur in three periods, from 2015–2016 (upper panel) to 2017–2018 (lower panel). Vertical lines mark the moments of spectral observations.

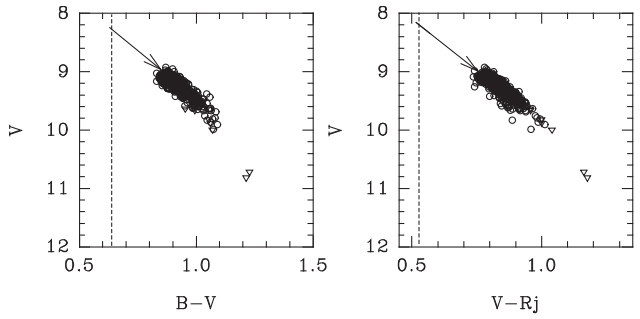

Figure 3. Colour–magnitude diagrams for SU Aur, where open circles denote the Majdanak data of 1983–2003 and triangles denote CrAO photometry during the miminum of 2017. Arrows indicate the slope of the interstellar reddening. Vertical dashed lines mark the normal colours of a star with $T_{\rm eff} = 5945$ K.

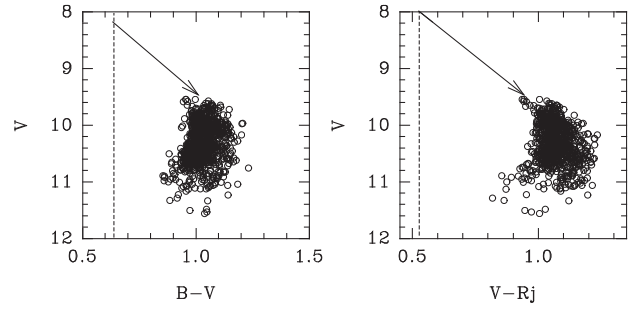

Figure 4. Colour–magnitude diagrams for RY Tau according to the Majdanak data of 1984–2004. Arrows indicate the slope of the interstellar reddening. Vertical dashed lines mark the normal colours of a star with $T_{\rm eff} = 5945$ K.

presented in Tables A1 and A2 for RY Tau and SU Aur, respectively. If we had no photometric observation for the date of the spectral observation, then the V magnitude was taken either from AAVSO data or from linear interpolation between the nearest dates in the photometric series. The probable error of the interpolated V mag was roughly estimated as 0.1 mag, taking into account the typical gradients in the light curves. The results of the NIR photometry for both stars are given in Tables A3 and A4, where we include visual photometry, when available for the dates of NIR photometry. Our previous NIR photometry of RY Tau in the period 1981–1997 is also included in Table A3.

4 RESULTS

4.1 Photometry

We start the analysis of the observations with a revision of the basic stellar parameters of RY Tau and SU Aur. From optical photometry, we estimate the interstellar extinction A_v and we calculate the absolute magnitude M_V. We adopt $T_{\rm eff} = 5945 \pm 140$ K (Calvet et al. 2004), which corresponds to spectral type G1–G2 IV. Then, with $T_{\rm eff}$ and M_V, we use the PMS models by Siess, Dufour & Forestini (2000) and we obtain the stellar luminosity, mass, radius and age.

In Figs 3 and 4, we plot colour–magnitude diagrams using the most extended and uniform photometric data collected at the Majdanak observatory over 20 yr (Grankin et al. 2007). The brightest V magnitudes ($V_{\rm max}$) in the diagrams supposedly represent the normal brightness of the star, when not obscured by circumstellar matter. We use $(V - R_{\rm j})$ colours to estimate the interstellar reddening. A star with $T_{\rm eff} = 5945$ K has an intrinsic colour of $(V - R_{\rm j}) = 0.52$ mag (Kenyon & Hartmann 1995). The unreddened V magnitudes, corresponding to the intrinsic $(V - R_{\rm j})$ colour, are $V = 8.20$ mag for SU Aur and $V = 8.00$ mag for RY Tau, as indicated by the cross-section of the reddening lines with the dashed lines. With an error of the adopted $T_{\rm eff}$ of about 142 K and the scatter of points in the $V/(V - R_{\rm j})$ diagrams, the error of the unreddened V might be within 0.10 mag. From these estimates, we obtain the interstellar reddening $A_v = 0.80 \pm 0.10$ mag for SU Aur and $A_v = 1.60 \pm 0.10$ mag for RY Tau. These values are consistent with previous estimates of the reddening from optical data (e.g. Calvet et al. 2004; Herczeg & Hillenbrand 2014; Grankin 2017).

The diagrams of RY Tau show a reversal of colours: as the circumstellar extinction becomes large, the colour turns bluer. The colour reversal effect is typical for UX Ori type stars: obscuration of star by the circumstellar dust results in an increased contribution of the light scattered on the dust particles. This effect was earlier observed in some cTTSs (e.g. RY Lup; Gahm et al. 1989, 1993b). In RY Tau, we do not see the linear part of the $V/(B - V)$ diagram but only the curved track, which might mean that the star still remains obscured by circumstellar dust even at the brightest state. Therefore, in the case of RY Tau, the estimated A_V can be considered only as an upper limit of interstellar reddening. In SU Aur, this effect is normally absent. The resulting stellar parameters are given in Table 1.

The pattern of light variability of RY Tau and SU Aur can be illustrated with the SED in the optical and NIR regions, covered by our photometry (see Tables A3 and A4). We selected a few observations at high and low brightness in the V band of each star. The corresponding SEDs are shown in Figs 5 and 6. In both stars, the SED is a sum of the stellar radiation reddened by the interstellar and circumstellar extinctions and a blackbody radiation of the circumstellar dust. The difference between the two stars is the relative contribution of the stellar and circumstellar radiation. In RY Tau, the optical part of the SED is more depressed by the large circumstellar extinction. At minimal brightness, the optical SED is more flat because of the light scattered by the circumstellar dust. There is a small but noticable variability in the NIR part of the SED in both stars.

4.2 Spectroscopy

In the analysis of the spectral series, we focus on variations of the Hα and Na I D line profiles, which are the strongest indicators of gas flows in the visible region of the spectrum. In addition, some other lines, including photospheric lines, were involved in the analysis. Our spectroscopic series cover a major part of the light variations: $V = 9.8$–11.2 mag in RY Tau and $V = 9.3$–10.8 mag in SU Aur. In both stars, the photospheric spectrum remains unchanged: the depth of the photosphere lines in the region around 6000 Å at high and low brightness remains the same within ± 2 per cent of the continuum level. This means that the observed light variations are not related to any surface phenomenon, such as hotspots or cool spots, but they are mostly due to variable circumstellar extinction. The stellar radial velocity is $+18.0 \pm 2.0$ km s^{-1} in both RY Tau and SU Aur, consistent with previous measurements (Petrov et al. 1996, 1999).

The most evident result is the large variability in Hα and Na I D profiles on a time-scale of a day and longer. Samples of typical line profiles in RY Tau are shown in Fig. 7. In this and other diagrams of spectral lines, we use the astrocentric radial velocity scale. The

Table 1. Stellar parameters of RY Tau and SU Aur.

Star	Distance (pc)	V_{max} (mag)	A_v (mag)	M_v (mag)	T_{eff} [a] (K)	$L/L_\odot$	$R/R_\odot$	$M/M_\odot$	Age (Myr)
RY Tau	150.0 ± 10	9.55	1.60	2.11 ± 0.15	5945.0 ± 142.5	13.50 ± 1.70	3.30 ± 0.25	2.08 ± 0.10	$4.70^{+1.00}_{-0.80}$
SU Aur	142.4 ± 12	8.95	0.80	2.43 ± 0.18	5945.0 ± 142.5	10.09 ± 1.64	2.85 ± 0.22	1.88 ± 0.10	$6.60^{+1.04}_{-0.82}$

[a] T_{eff} is taken from Calvet et al. (2004).

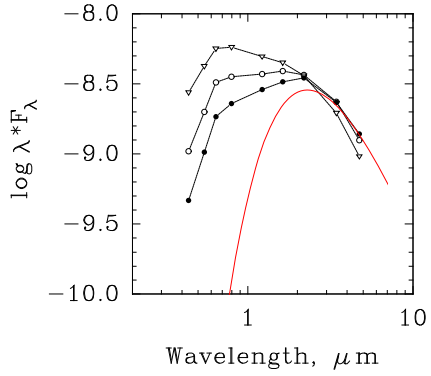

Figure 5. SEDs of SU Aur, corresponding to $V = 9.18$ (triangles), $V = 10.00$ (open circles) and $V = 10.72$ (filled circles). The solid curve is the SED of a blackbody at $T = 1600$ K. Flux F_λ is expressed in units of erg cm^{-2} s^{-1} Å^{-1}.

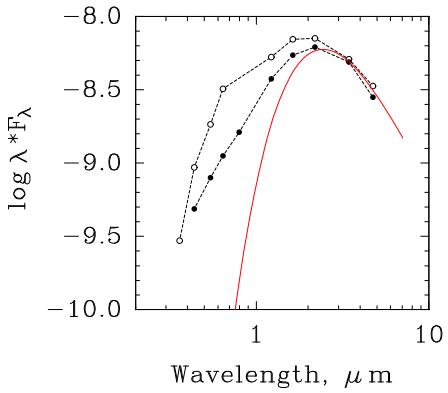

Figure 6. SEDs in RY Tau, corresponding to $V = 10$ (open circles) and $V = 11$ (filled circles). The solid curve is the SED of a blackbody at $T = 1500$ K. Flux F_λ is expressed in units of erg cm^{-2} s^{-1} Å^{-1}.

Hα line is in broad emission extending from -300 to $+300$ km s^{-1}, with a strong central depression at about -100 km s^{-1}, which often extends further to the blue and, in rare cases, drops even below continuum. In terms of line profile classification by Reipurth, Pedrosa & Lago (1996), Hα is of II-B type most of the time. This is characteristic of an outflow, probably a disc wind (Kurosawa et al. 2011) or conical wind (Kurosawa & Romanova 2012). However, a redshifted depression in the Hα profile at $+100$ to $+200$ km s^{-1} is often present. Comparison of the concurrent Hα and Na I D line profiles in Fig. 7 clearly shows that the depressions in the Hα profile correspond to real absorption components in the Na I D lines, although at a lower range of velocities. Therefore, the redshifted absorption in both lines forms in the infalling gas, most probably in the accretion funnels. These redshifted absorptions, indicating accretion, are much better seen in the Pashen and Brackett series as real absorption below the continuum (e.g. Folha & Emerson 2001). In our analysis of the Hα profile variability, we study only the outflow activity.

In SU Aur, the Hα profiles show similar features of wind and accretion (Fig. 8). The central absorption at about -40 km s^{-1} is more narrow and deep, and another broader absorption appears sometimes at radial velocities of -100 to -250 km s^{-1}. The same features are present in the Na I D lines, which consist of broad photospheric absorption, narrow interstellar absorption and the variable blueshifted absorption that indicates outflow.

4.2.1 *Spectral series of RY Tau*

The Hα emission is an indicator of MHD processes at the boundary between the stellar magnetosphere and the accretion disc. The stellar brightness is related to the amount of dust around the star. In the following analysis, we seek a possible connection between variations in Hα emission and in the circumstellar extinction (i.e. the stellar brightness).

The range of Hα profile variability in RY Tau is shown in Fig. 9. The most variable part of the Hα profile is the central peak of emission at about $+50$ km s^{-1}and the depression in the blue wing at about -100 to -200 km s^{-1}. In order to quantify the profile variability, we measured equivalent widths (EWs) in three ranges of the velocity scale: EWb at -200 to -100 km s^{-1}, EW0 at -100 to 0 km s^{-1} and EWr at 0 to $+100$ km s^{-1}. The ratio EWb/EWr (or EW0/EWr) is a measure of the line asymmetry, caused mostly by the outflow. Fig. 10 shows the relation between the Hα profile asymmetry and stellar brightness V. In the first two periods, when the line profile was most variable, there was a clear correlation: the blue wing of Hα emission was depressed at the moments of high brightness of the star. Consequently, the circumstellar extinction was lower during times of enhanced outflow. In the last two periods, when the activity resumed after the period of quiescence, the most variable part of the line profile shifted to lower velocities, and the ratio EW0/EWr showed a correlation with stellar brightness.

4.2.2 *Spectral series of SU Aur*

SU Aur was monitored only during three periods. The range of Hα profile variability is shown in Fig. 11. The line is broad with wings extending to radial velocities of about ± 400 km s^{-1}. On one occasion, the red emission wing extends to almost 600 km s^{-1}. Both wings vary in intensity, indicating irregular processes of accretion and outflows. There is a relatively stable narrow absorption at about -50 km s^{-1}. In terms of magnetospheric accretion and disc wind models, this can be identified with absorption in the disc wind or conical wind (Kurosawa et al. 2011; Kurosawa & Romanova 2012).

In the period 2016–2017, the star showed an unusually low intensity in the Hα emission line. The mean level of stellar brightness did not change considerably in that period, so it was a real decrease in the Hα flux. In the Na I D lines, the absorption related to outflow was absent on some nights of that period. Interestingly, in

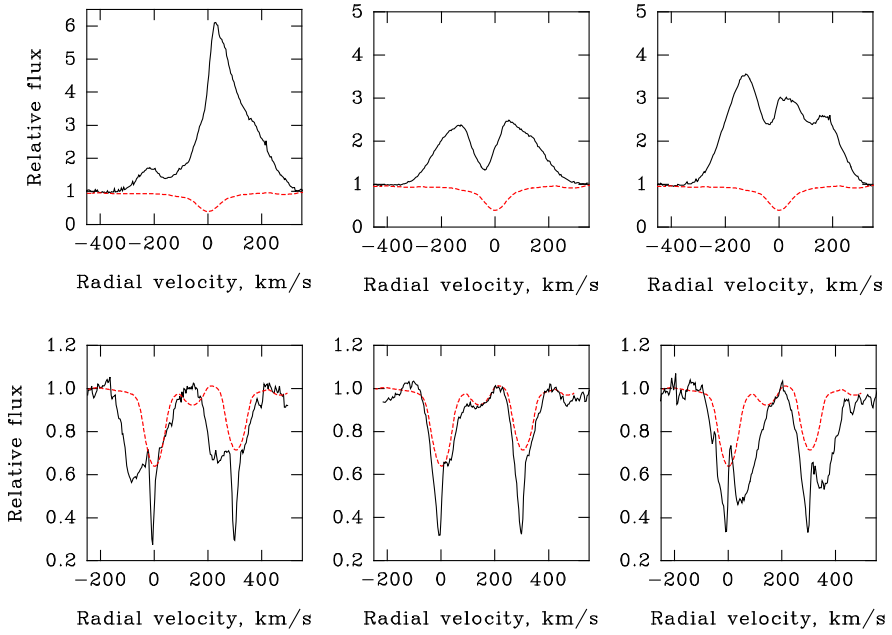

Figure 7. Sample of line profiles in RY Tau. The upper panels show Hα and the lower panels show Na I D. The columns show HJD = 245 6993.262, 245 7799.442 and 245 7091.204 from left to right. The dashed curves are for the template G2 V star, $v \sin i = 50$ km s^{-1}.

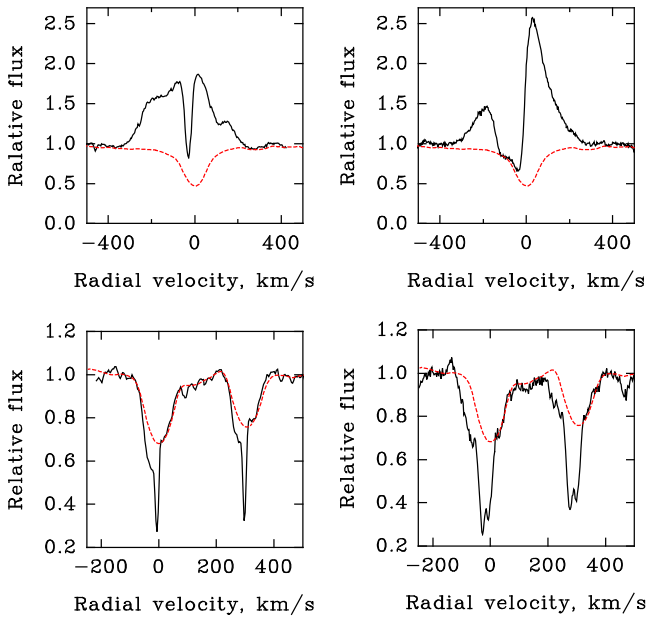

Figure 8. Sample of line profiles in SU Aur. The upper panels show Hα and the lower panels show Na I D. The left and right columns are for HJD = 245 8030.503 and 245 8166.352, respectively. The dashed curves are for the template G2 V star, $v \sin i = 66$ km s^{-1}.

2016–2017, the star also showed an unusual low amplitude in the brightness variations (Fig. 2, middle panel). Unlike RY Tau, there is no correlation between the Hα line asymmetry and the stellar brightness in SU Aur.

4.2.3 Hα flux variations

So far, we have analysed the Hα EW and the line profile. In the following discussion, an important parameter is the flux radiated in Hα. Our photometry enables us to transform the Hα EW into flux: $F = EW \times 10^{-0.4\times(V-V_0)}$, where V_0 is a reference level of stellar brightness (e.g. $V_0 = 10$ mag). In this case, the flux is expressed in units of the continuum flux density of a star with $V = 10$ mag, which is 3.67×10^{-13} erg cm^{-2} s^{-1} Å^{-1}. The photometric R band is more appropriate for Hα flux calibration, but for some spectral observations only V is available from the AAVSO data. In RY Tau, the colour $(V - R)$ does not change considerably with brightness (see Fig. 4); on average, $(V - R) = 1.1 \pm 0.1$ mag. The use of V magnitudes introduces a constant factor to the flux adding a relative error of about 10 per cent. In our analysis, the absolute value of the flux is not critical.

Time variations of the absolute flux in Hα emission line in RY Tau and SU Aur are shown in Fig. 12.

5 DISCUSSION

The photometric and spectral properties of RY Tau and SU Aur, discussed in the previous sections, reveal similarities and differences between the two PMS stars. Stellar parameters are about the same, but RY Tau is younger and more obscured by the circumstellar dust.

The powerful outflows in cTTSs are driven by accretion, and the observed variations of the outflows are related to the unstable MHD processes at the boundary between the inner disc and stellar magnetosphere (Zanni & Ferreira 2013). In the observed Hα profiles, the most stable feature is the central absorption at -100 to -50 km s^{-1}. This absorption is related to an extended disc wind in the case of high inclinations (50°–80°) of its rotational axis to the line of sight (Kurosawa et al. 2011). The relative stability of this feature is due to a large area along the line of sight above the disc plane, where the absorption is formed. Alternatively, a similar type of profile can be formed in a conical wind starting near the interface of the magnetosphere and the accretion disc, when the stellar dipole magnetic field is compressed by the accretion disc into an X-wind-like configuration (Kurosawa & Romanova 2012).

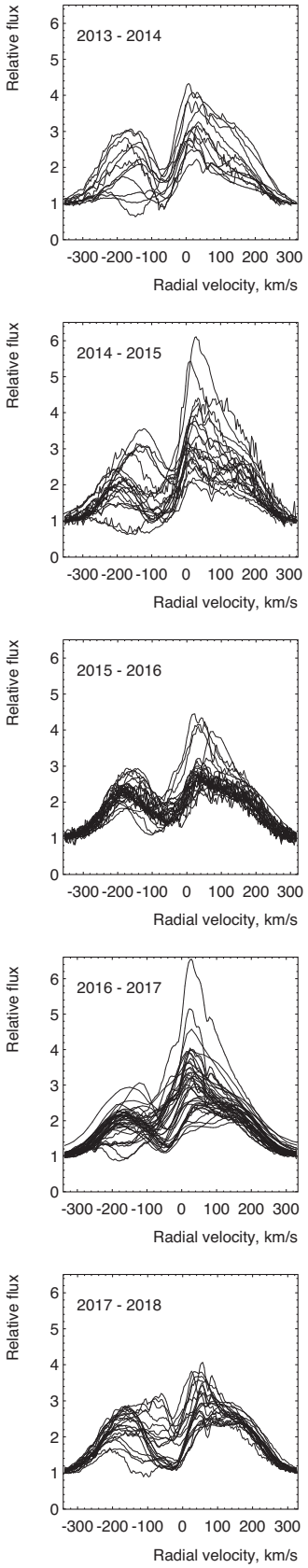

Figure 9. Hα profile variation in RY Tau in five periods, as indicated in the upper-left corner of each panel. The high activity in 2014–2015 changed to a period of quiescence in 2015–2016.

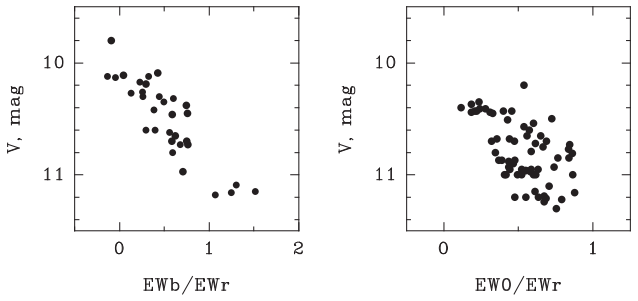

Figure 10. Relation between the stellar brightness V and the Hα line asymmetry. Left panel: data of 2013–2015. Right panel: data of 2016–2018. The star is brighter when the line asymmetry indicates stronger wind.

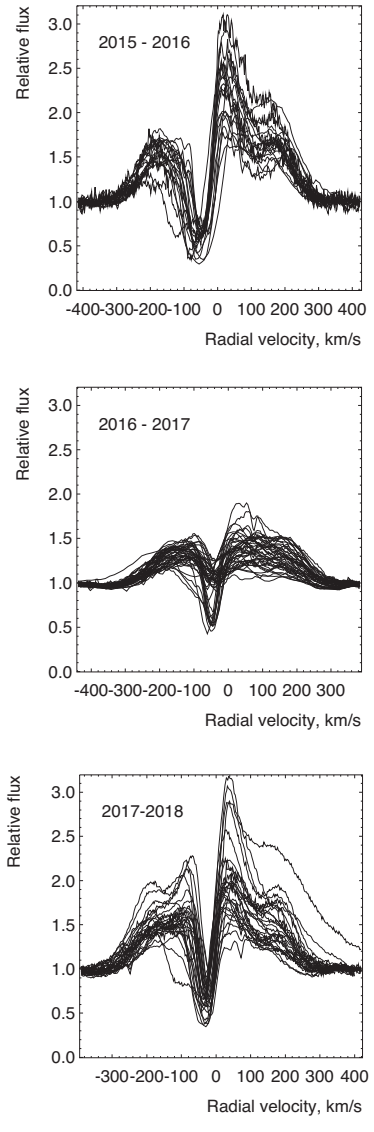

Figure 11. Hα profilevariation in SU Aur in three periods. The observation period is indicated in the upper-left corner of each plot.

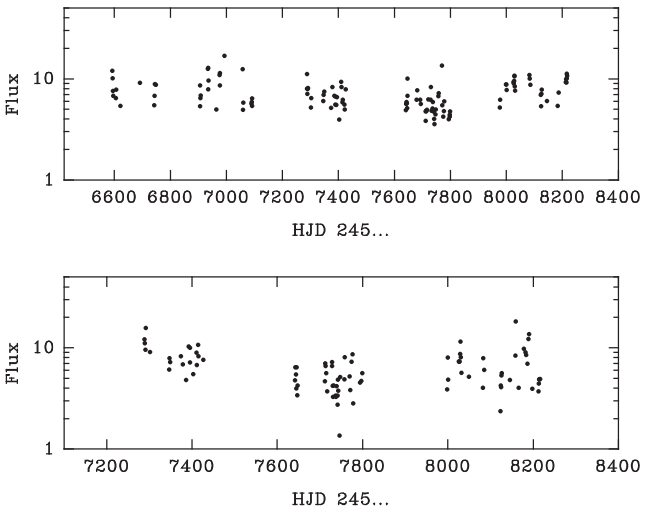

Figure 12. Time variations in the absolute flux in he Hα emission line. The upper and lower panels show RY Tau and SU Aur, respectively. Flux is in units of 3.67×10^{-13} erg cm^{-2} s^{-1} Å^{-1}.

The blue wing of Hα emission is more variable at -200 to -100 km s^{-1}. The amplitude of the flux variation in that region is large, including the occasional appearance of the classical P Cyg type profile. Such profiles indicate radially expanding outflows, which are drastically different from the disc wind. This fast expansion can be identified with a magnetospheric ejection (ME). The MEs appear when the inner disc comes closer to the star and the faster Keplerian rotation twists the stellar magnetosphere in the azimuthal direction, which results in cyclically repeated openings and reconstructions of the magnetosphere (Goodson et al. 1997; Zanni & Ferreira 2013).

The wind dynamics and variations in the circumstellar extinction are more evident in RY Tau. This could be a consequence of the higher accretion rate. The mass accretion rate can be estimated from the EWs of the hydrogen and helium emission lines, using the empirical relations between line luminosity and mass accretion rate (e.g., Alcala et al. 2014). We derived the average accretion rates of our targets as $\approx 3.6 \times 10^{-8}$ M$_\odot$ yr^{-1} for RY Tau and $\approx 4 \times 10^{-9}$ M$_\odot$ yr^{-1} for SU Aur. This is consistent with the previous determinations of the mass accretion rates from optical–UV data on these stars (Calvet et al. 2004).

In the following discussion, we consider two topics: the influence of the MEs on the dusty disc wind, and the nature of the gradual changes in the wind activity on a time-scale of 1–2 yr.

5.1 Interaction between the wind and the dusty environment

The observed decrease of circumstellar extinction at the moments of the most intensive MEs (see Fig. 10) in RY Tau provides a possibility to localize the dust responsible for the extinction. Our observations show that the characteristic radial velocity of the MEs is about 200 km s^{-1}, and the characteristic time-scale of MEs is about 2 d (Babina et al. 2016) . Then, the typical distance from the expanding magnetosphere to the obscuring dust screen must be about 0.2 au. Assuming a magnetospheric radius of about 5 stellar radii (= 0.08 au) we obtain the location of the dust screen at about 0.3 au. This is near the inner edge of the dusty disc, where the dust temperature is high. The SED in the NIR (Fig. 6) shows radiation of dust at $T = 1500$ K. Therefore, this hot dust can be identified as a cause of the variable circumstellar extinction. The star is seen through the dust screen, where the circumstellar extinction on a line of sight is changing, while the bulk radiation from the dust remains relatively constant. A similar effect was observed in another cTTS, namely RW Aur. During a deep minimum of optical brightness of the star, the NIR radiation increased, thus indicating the appearance of hot dust (Shenavrin, Petrov & Grankin 2015).

An accretion disc is a reservoir of dust. Coarse dust grains are concentrated at the disc plane, while small particles are present in the disc atmosphere and can be elevated from the disc plane by dynamical pressure of the disc wind (Safier 1993). The disc wind is most intensive at the inner part of the disc, where the temperature is higher. Therefore, the most dense dust screen is formed at the inner disc, near the dust sublimation distance and further out from the star.

The disc wind flows along the open magnetic field lines of the disc. The observed correlation between the Hα profile variations and stellar brightness (Fig. 10) implies that there must be a physical mechanism of interaction between the MEs and the dusty disc wind close to the magnetosphere. As a tentative explanation, we suggest that a parcel of ionized gas, ejected from magnetosphere, can affect the magnetic field of the inner disc and thus temporarily change the disc wind flow on the line of sight.

In RY Tau, this effect was more pronounced during the two periods of maximal activity of magnetospheric ejections in 2013–2015. Then, the star entered a period of quiescence, when both the wind activity and the light variations became lower. In the last two periods, the effect appeared again. As this effect has been observed repeatedly for several years, it can be considered as well established. In SU Aur, such a connection between the wind and the circumstellar extinction was not observed.

The colour–magnitude diagrams (Fig. 4) show that RY Tau is permanently hidden by the dust screen, so that the intensity of the light scattered on the dust particles is comparable to the intensity of the direct star light. Contrary to RY Tau, SU Aur is at normal (high) brightness most of the time, but is occasionally obscured by circumstellar dust. This difference might be related to age: RY Tau is younger and possesses a more massive accretion disc (Akeson et al. 2005).

5.2 Seasonal changes in outflow activity

Our results show that there is a gradual change of the outflow activity on time-scales of a few years. In RY Tau, we observed a period of activity in the first two periods, which was then replaced by a period of quiescence between 2015 and 2016. Although the number of observations in that period were large, the Hα emission showed only a small amplitude of variability. A similar drop of activity was observed in SU Aur between 2016 and 2017. Obviously, in the periods of quiescence, the mechanism of ME did not work.

The period of quiescence in SU Aur, when the disc wind became very weak and almost absent, is remarkable. Fig. 13 shows that the usually strong central absorption in Hα almost disappeared in 2016 December. The corresponding absorption feature in the sodium doublet disappeared completely: the Na I D2 line showed only broad photospheric absorption and a narrow interstellar feature. The period when the wind was weak started in 2016 November and lasted to the end of the period. At the beginning of the next period (2017 September), the wind was active again. The minimal EW of Hα reached 0.5–1.0 Å and the corresponding accretion rate was less than 10^{-9} M$_\odot$ yr^{-1}. Interestingly, during the quiescence period, SU Aur was also quiet photometrically, with a minimal circumstellar extinction and low variability within $V = 9.2$–9.4 (see Fig. 2, middle panel).

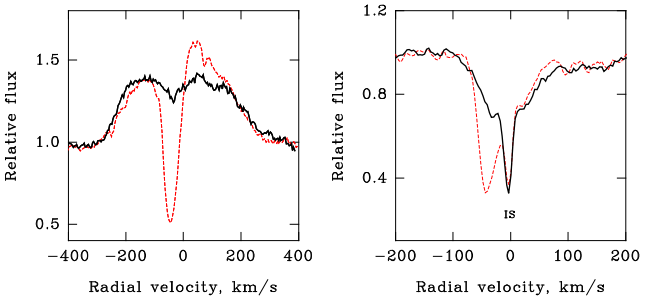

Figure 13. Disappearance of the wind features in SU Aur in 2016 December, for Hα (left panel) and Na I D2 (right panel). The dashed lines are typical profiles with blueshifted wind absorptions. The solid lines show the spectrum of 2016 December 05. IS denotes interstellar absorption in the D2 line.

The outflow is accretion-driven, and the region of most unstable outflow is the interface between the disc and stellar magnetosphere. Could the quiescence periods be a consequence of a temporal lowering of the accretion rate? The absolute flux in the Hα line is often used as a measure of the mass accretion rate. Fig. 12 shows that the instant accretion rate is highly variable, while the average level does not change significantly from period to period. From the five periods of our observations of RY Tau, we do not see a correlation between the wind activity and the average Hα flux in a period. The quiescent period in 2015–2016 corresponds to an average level of the Hα flux. In SU Aur, we have only three periods of observations, so it is difficult to make a conclusion. The period of quiescence in 2016–2017 corresponds to a slightly lower Hα flux level.

Another important parameter is the stellar magnetic field, which truncates the accretion disc. Zeeman Doppler imaging of cTTSs shows a multipolar structure of magnetic fields (Johnstone et al. 2014, and references therein). Apart from the stellar mass and mass accretion rate, the truncation radius of the accretion disc is primarily determined by the strength of the dipole component of the field. If there is a solar-like magnetic cycle in a cTTS, then we would expect cyclic variations of the disc truncation radius (Johnstone et al. 2014).

Typically, the truncation radius is within the radius of corotation. In this case, the inner disc rotates faster than the stellar magnetosphere, and the regime of MEs becomes possible (Zanni & Ferreira 2013). In case of a stronger dipole component of the stellar magnetic field, the disc is truncated outside the corotation radius and the propeller regime is activated (Romanova et al. 2009).

The strength and topology of the magnetic field in cTTSs vary on a time-scale of years (e.g., Donati et al. 2011, 2012). We suggest that the observed changes of the outflow activity in our targets, including the periods of quiescence, might be related to a slow variation of the global stellar magnetic fields, regardless of the type of wind. RY Tau and SU Aur are fast rotating stars with radiative cores and convective envelopes, so the generation of the stellar magnetic field might be similar to the solar one. Spectral monitoring of the Hα profile variability in selected cTTSs over several years could potentially reveal cycles of magnetic activity, if any.

6 CONCLUSIONS

(i) RY Tau and SU Aur have nearly the same stellar parameters, but different circumstellar environments. RY Tau is younger, with a higher accretion rate and a more massive accretion disc. In both stars, the light variability in the optical region is mostly due to the circumstellar extinction.

(ii) The dusty screen responsible for the variable circumstellar extinction of RY Tau is located at the inner edge of the accretion disc; this is a dusty disc wind. The obscuring dust has a temperature of about 1500 K. The circumstellar extinction in the line of sight is variable, while the NIR radiation from the bulk of the dust remains about the same.

(iii) In RY Tau, the dusty screen permanently obscures the star; the star is never seen free of foreground dust. Unlike RY Tau, SU Aur exhibits a moderate circumstellar extinction most of the time, with rare cases where light drops due to more extinction.

(iv) In RY Tau, we discovered a new effect: during the events of enhanced outflow, the cicumstellar extinction becomes lower. This indicates that outflows can affect the inner dusty wind.

(v) In both RY Tau and SU Aur, we detected periods of quiescence: lower amplitude variations in the Hα line profiles. The quiescence periods lasted for about 1 yr.

ACKNOWLEDGEMENTS

This research was supported by the RFBR grant 16-02-00140. It was based partly on observations made with the Nordic Optical Telescope, operated by the Nordic Optical Telescope Scientific Association at the Observatorio del Roque de los Muchachos, La Palma, Spain, of the Instituto de Astrofisica de Canarias, using ALFOSC, which is provided by the Instituto de Astrofisica de Andalucia (IAA) under a joint agreement with the University of Copenhagen and NOTSA.

We acknowledge support from a Visitors Programme at the Department of Astronomy at Stockholm University. JFG and RMGA were supported by Fundação para a Ciência e a Tecnologia (FCT) through national funds (UID/FIS/04434/2013) and by FEDER through COMPETE2020 (POCI-01-0145-FEDER-007672). RMGA is supported by the fellowship PD/BD/113745/2015, under the FCT PD Program PhD::SPACE, funded by FCT (Portugal) and POPH/FSE (EC) and by CRUP through a cooperation programme (PAULIF: TC-16/17). DEM acknowledges his work as part of the research activity supported by the National Astronomical Research Institute of Thailand (NARIT), Ministry of Science and Technology of Thailand. SYuG was supported in part by the Ministry of Education and Science of Russia (the basic part of the Stateassignment, RK no. AAAA-A17-117030310283-7) and by the Act no. 211 of the Government of the Russian Federation, agreement № 02.A03.21.0006.

We acknowledge with thanks the variable star observations from the AAVSO International Database contributed by observers worldwide and used in this research.

This work has made use of data from the European Space Agency (ESA) mission *Gaia* (https://www.cosmos.esa.int/gaia), processed by the *Gaia* Data Processing and Analysis Consortium (DPAC; https://www.cosmos.esa.int/web/gaia/dpac/consortium). Funding for the DPAC has been provided by national institutions, in particular the institutions participating in the *Gaia* Multilateral Agreement.

PPP thanks Marina Romanova for valuable comments.

REFERENCES

Agra-Amboage V., Dougados C., Cabrit S., Garcia P. J. V., Ferruit P., 2009, A&A, 493, 1029
Akeson R. L. et al., 2005, ApJ, 622, 440
Akitaya H., Ikeda Y., Kawabata K. S., Matsuda K., Okazaki A., Seki M., 2009, A&A, 499, 163
Alcala J. M. et al., 2014, A&A, 561, 2
Alencar S. H. P., Basri G., 2000, AJ, 119, 1881

Alonso-Martinez M., Riviere-Marichalar P., Meeus G., Kamp I., Fang M., Podio L., Dent W. R. F., Eiroa C., 2017, A&A, 603, 138
Ardila D. R., Basri G., Walter F. M., Valenti J. A., Johns-Krull C. M., 2002, ApJ, 567, 1013
Babina E. V., Artemenko S. A., Petrov P., 2016, Astron. Rep., 42, 193
Basri G., Martin E. L., Bertout C., 1991, A&A, 252, 625
Blandford R. D., Payne D. G., 1982, MNRAS, 199, 883
Bouvier J., Alencar S. H. P., Harries T. J., Johns-Krull C. M., Romanova M. M., 2007, in Reipurth B., Jewitt D., Keil K., eds, Protostars and Planets V. Univ. of Arizona Press, Tuscon, AZ, p. 479
Bouvier J., Bertout C., Bouchet P., 1988, A&AS, 75, 1
Bouvier J., Cabrit S., Fernandez M., Martin E. L., Matthews J. M., 1993, A&A, 272, 176
Cabrit S., Edwards S., Strom S. E., Strom K. M., 1990, ApJ, 354, 687
Calvet N., Muzerolle J., Briceño C., Hernández J., Hartmann L., Saucedo J. L., Gordon K. D., 2004, AJ, 128, 1294
Camenzind M., 1990, Rev. Mod. Astron., 3, 234
Chou M-Y. et al., 2013, AJ, 145, 108
Cody A. M., Tayar J., Hillenbrand L., Matthews J. M., Kallinger T., 2013, AJ, 145, 79
Cranmer S. R., 2009, ApJ, 706, 824
De Leon J. et al., 2015, ApJ, 806, L10
DeWarf L. E., Sepinsky J. F., Guinan E. F., Ribas I., Nadalin I., 2003, ApJ, 590, 357
Donati J. et al., 2012, MNRAS, 425, 2948
Donati J. F. et al., 2011, MNRAS, 412, 2454
Elias J. H., 1978, ApJ, 224, 857
Folha D. F. M., Emerson J. P., 2001, A&A, 365, 90
Furlan E. et al., 2011, ApJS, 195, 3
Gahm G. F., Fischerstrom C., Liseau R., Lindroos K. P., 1989, A&AS, 211, 115
Gahm G. F., Gullbring E., Fischerstrom C., Lindroos K. P., Loden K., 1993a, A&AS, 100, 371
Gahm G. F., Liseau R., Gullbring E., Hartstein D., 1993b, A&AS, 279, 477
Gaia Collaboration et al.2016a, A&A, 595, A2
Gaia Collaboration et al.2016b, A&A, 595, A1
Ghosh P., Lamb F. K., 1979, ApJ, 234, 296
Giampapa M. S., Basri G. S., Johns C. M., Imhoff C., 1993, ApJS, 89, 321
Gomez de Castro A. I., Marcos-Arenal P., 2012, ApJ, 749, 190
Gomez de Castro A. I., Verdugo E., 2007, ApJ, 654, L91
Goodson A. P., Winglee R. M., Böhm K.-H., 1997, ApJ, 489, 199
Grankin K. N., 2017, in Mickaelian A. M., Harutyunian H. A., Nikoghosyan E. H.eds, ASP Conf Ser. Vol. 37, Non-Stable Universe: Energetic Resources, Activity Phenomena, and Evolutionary Processes. Astron. Soc. Pac., San Francisco, p. 511
Grankin K. N., Melnikov S. Y., Bouvier J., Herbst W., Shevchenko V. S., 2007, A&A, 461, 183
Grinin V. P., Tambovtseva L. V., Weigelt G., 2012, A&A, 544, A45
Guilloteau S., Dutrey A., Piétu V., Boehler Y., 2011, A&A, 529, A105
Hamann F., Persson S. E., 1992, ApJS, 82, 247
Hartigan P., Edwards S., Ghandour L., 1995, ApJ, 452, 736
Hartmann L., Herczeg G., Calvet N., 2016, ARA&A, 54, 135
Herbst W., Herbst D. K., Grossman E. J., Weinstein D., 1994, AJ, 108, 1906
Herbst W., Koret D. L., 1988, AJ, 96, 1949
Herbst W., Shevchenko V. S., 1999, AJ, 118, 1043
Herbst W., Stine P. C., 1984, AJ, 89, 1716
Herbst W. et al., 1987, AJ, 94, 137
Herczeg G. J., Hillenbrand L. A., 2014, ApJ, 786, 97
Isella A., Carpenter J. M., Sargent A. I., 2010, ApJ, 714, 1746
Ismailov N. Z., Adigezalzade H. N., Bahaddinova G. R., 2015, Publication of Korean Astronomical Society, 30, 229
Jeffers S. V., Min M., Canovas H., Rodenhuis M., Keller C. U., 2014, A&A, 561, A23
Johns-Krull C. M., 1996, A&A, 306, 803
Johns C. M., Basri G., 1995, AJ, 109, 2800
Johnson H. L., Mitchell R. I., Iriarte B., Wisniewski W. Z., 1966, Communications of the Lunar and Planetary Laboratory, 4, 99
Johnstone C. P., Jardine M., Gregory S. G., Donati J. F., Hussain G., 2014, MNRAS, 437, 3202
Kafka S., 2017, Observations from the AAVSO International Database (https://www.aavso.org)
Kenyon S. J., Hartmann L., 1995, ApJS, 101, 117
Koenigl A., 1991, ApJ, 370, L39
Koornneef J., 1983, A&A, 128, 84
Kurosawa R., Harries T. J., Symington N. H., 2005, MNRAS, 358, 671
Kurosawa R., Romanova M. M., 2012, MNRAS, 426, 2901
Kurosawa R., Romanova M. M., Harries T. J., 2011, MNRAS, 416, 2623
Loinard L., Torres R. M., Mioduszewski A. J., Rodríguez L. F., González-López lira R. A., Lachaume R., Vázquez V., González E., 2007, ApJ, 671, 546
Matt S., Pudritz R. E., 2005, ApJ, 632, L135
Mendigutía I., Eiroa C., Montesinos B., Mora A., Oudmaijer R. D., Merín B., Meeus G., 2011, A&A, 529, A34
Millan-Gabet R., Malbet F., Akeson R., Leinert C., Monnier J., Waters R., 2007, in Reipurth B., Jewitt D., Keil K., eds, Protostars and Planets V. Univ. of Arizona Press, Tuscon, AZ, p. 539
Muzerolle J., Calvet N., Hartmann L., D'Alessio P., 2003, ApJ, 597, L149
Nguyen D. C., Brandeker A., van Kerkwijk M. H., Jayawardhana R., 2012, ApJ, 745, 119
Oliveira J. M., Foing B. H., van Loon J. T., Unruh Y. C., 2000, A&A, 362, 615
Panchuk V. E., Yushkin M. V., Yakopov M. V., 2011, Astrophysical Bulletin, 66, 355
Petrov P. P., 1990, Ap&SS, 169, 61
Petrov P. P., 2003, Astrophysics, 46, 506
Petrov P. P., Gullbring E., Ilyin I., Gahm G. F., Tuominen I., Hackman T., Loden K., 1996, A&A, 314, 821
Petrov P. P., Zajtseva G. V., Efimov Y. S., Duemmler R., Ilyin I. V., Tuominen I., Shcherbakov V. A., 1999, A&A, 341, 553
Pudritz R. E., Norman C. A., 1986, ApJ, 301, 571
Reipurth B., Pedrosa A., Lago M. T. V. T., 1996, A&AS, 120, 229
Romanova M. M., Long M., Kulkarni A. K., Kurosawa R., Ustyugova G. V., Koldoba A. K., Lovelace R. V. E., 2007, in Bouvier J., Appenzeller I., eds, Proc. IAU Symp. Vol. 243, Star–Disk Interaction in Young Stars, Kluwer, Dordrecht, p. 277
Romanova M. M., Owocki S. P., 2015, Space Sci. Rev., 191, 339
Romanova M. M., Ustyugova G. V., Koldoba A. V., Lovelace R. V. E., 2009, MNRAS, 399, 1802
Safier P. N., 1993, ApJ, 408, 115
Schegerer A. A., Wolf S., Ratzka T., Leinert C., 2008, A&A, 478, 779
Shenavrin V. I., Petrov P. P., Grankin K. N., 2015, Information Bulletin on Variable Stars, 6143, 1
Shenavrin V. I., Taranova O. G., Nadzhip A. E., 2011, Astronomy Reports, 55, 31
Shu F., Najita J., Ostriker E., Wilkin F., Ruden S., Lizano S., 1994, ApJ, 429, 781
Siess L., Dufour E., Forestini M., 2000, A&A, 358, 593
Skinner G. L., Schneider P. C., Audard M., Gudel M., 2018, ApJ, 855, 143
Skinner S. L., Audard M., Gudel M., 2016, ApJ, 826, 84
Smith K., Audard M., Gudel M., Skinner S., Pallavicini R., 2005, in Favata F., Hussain G. A. J., Battrick B., eds, ESA Special Publication Vol. 560, 13th Cambridge Workshop on Cool Stars, Stellar Systems and the Sun, ESA Publications Division, Noordwijk, p. 971
Smith K. W., Lewis G. F., Bonnell I. A., Bunclark P. S., Emerson J. P., 1999, MNRAS, 304, 367
St-Onge G., Bastien P., 2008, ApJ, 674, 1032
Takami M. et al., 2013, ApJ, 772, 145
Unruh Y. C., Solanki S. K., Fligge M., 2000, Space Sci. Rev., 94, 145
Unruh Y. C. et al., 2004, MNRAS, 348, 1301
Vink J. S., Drew J. E., Harries T. J., Oudmaijer R. D., Unruh Y., 2005, MNRAS, 359, 1049
Zajtseva G., Petrov P., Ilyin I., Duemler R., Tuominen I., 1996, Information Bulletin on Variable Stars, 4408, 1
Zajtseva G. V., 2010, Astrophysics, 53, 212
Zajtseva G. V., Kolotilov E. A., Petrov P. P., Tarasov A. E., Shenavrin V. I., Shcherbakov A. G., 1985, Pisma v Astronomicheskii Zhurnal, 11, 271
Zanni C., Ferreira J., 2013, A&A, 550, A99

APPENDIX A: OBSERVATION DATA

Table A1. The *V* magnitudes of RY Tau for the dates of spectral observations. The Heliocentric Julian date (HJD) in the first column is followed by the site of the observation (CAHA, Calar Alto Observatory; CrAO, Crimean Astrophysical Observatory; NOT, Nordic Optical Telescope; TNO, Thai National Observatory), magnitude measured in the *V* band, corresponding error and source (CAS, Crimean Astronomical Station; AAVSO, American Association of Variable Star Observers; Int, value interpolated from AAVSO and CrAO photometry).

HJD 240 0000	Site	*V*	*V* error	Source of *V*
56592.444	CrAO	10.46	0.01	CrAO
56593.438	CrAO	10.70	0.01	CrAO
56594.340	CrAO	10.45	0.01	CrAO
56595.306	CrAO	10.38	0.01	CrAO
56605.436	CrAO	10.09	0.01	CrAO
56606.442	CrAO	10.11	0.01	CrAO
56621.318	CrAO	10.19	0.01	CrAO
56691.389	CrAO	9.87	0.01	AAVSO
56742.224	CrAO	10.68	0.10	Int
56743.185	CrAO	10.79	0.10	Int
56744.242	CrAO	10.91	0.10	Int
56748.291	CrAO	10.97	0.01	CrAO
56905.524	CrAO	10.29	0.01	CrAO
56906.520	CrAO	10.26	0.01	CrAO
56907.504	CrAO	10.30	0.10	Int
56908.509	CrAO	10.35	0.01	CrAO
56933.513	CrAO	10.13	0.10	Int
56934.475	CrAO	10.13	0.10	Int
56935.416	CrAO	10.12	0.01	CrAO
56936.415	CrAO	10.17	0.01	CrAO
56964.464	CrAO	10.32	0.01	CrAO
56975.442	CrAO	10.42	0.01	CrAO
56976.453	CrAO	10.60	0.01	CrAO
56977.468	CrAO	10.58	0.10	Int
56993.262	CrAO	10.27	0.01	CrAO
57058.188	CrAO	10.62	0.01	CrAO
57059.231	CrAO	10.76	0.01	AAVSO
57060.188	CrAO	10.78	0.10	Int
57089.231	CrAO	11.09	0.01	CrAO
57090.203	CrAO	11.18	0.01	CrAO
57091.204	CrAO	11.16	0.02	CrAO
57092.230	CrAO	11.15	0.08	CrAO
57287.438	CrAO	10.61	0.01	CrAO
57288.532	CrAO	10.61	0.01	CrAO
57289.438	CrAO	10.61	0.01	CrAO
57290.511	CrAO	10.69	0.01	CrAO
57291.444	CrAO	10.78	0.01	CrAO
57301.430	CrAO	10.64	0.01	CrAO
57302.482	CrAO	10.56	0.01	AAVSO
57346.369	CrAO	10.75	0.01	CrAO
57347.483	CrAO	10.68	0.01	CrAO
57349.166	TNO	10.75	0.01	AAVSO
57374.180	CrAO	10.74	0.01	CrAO
57378.300	CrAO	10.93	0.01	CrAO
57386.009	TNO	10.53	<0.01	AAVSO
57389.298	CrAO	10.80	0.01	AAVSO
57389.413	CAHA	10.80	0.01	AAVSO
57392.334	CrAO	10.78	0.01	CrAO
57403.056	TNO	10.50	0.10	Int
57410.370	CAHA	10.38	<0.01	AAVSO
57411.368	CAHA	10.40	0.10	Int
57414.380	CAHA	10.52	0.01	CrAO, CAS
57415.458	CAHA	10.59	0.10	Int
57421.302	CrAO	11.04	0.01	CrAO
57422.315	CrAO	11.04	0.10	Int
57426.327	CrAO	10.98	0.01	CrAO
57641.426	CrAO	10.96	0.01	CrAO, CAS
57642.442	CrAO	10.95	0.01	CrAO
57643.418	CrAO	10.91	0.01	CrAO, CAS
57644.402	CrAO	10.88	0.01	CrAO
57645.393	CrAO	11.01	0.01	CrAO
57646.416	CrAO	10.96	0.01	CrAO
57647.424	CrAO	10.97	0.01	CrAO
57679.618	NOT	10.93	<0.01	AAVSO
57681.607	NOT	11.07	0.10	Int
57691.681	NOT	11.20	0.10	Int
57694.607	NOT	11.06	0.02	AAVSO
57711.424	CrAO	11.31	0.01	CrAO
57712.387	CrAO	11.22	0.01	CrAO
57713.442	CrAO	11.16	0.01	CrAO
57714.418	CrAO	11.27	0.01	CrAO, CAS
57716.650	NOT	11.04	0.02	AAVSO
57721.578	NOT	11.02	0.10	Int
57728.594	NOT	11.16	0.01	CrAO, CAS
57730.459	NOT	11.15	0.01	CrAO
57732.546	NOT	11.15	0.10	Int
57736.650	NOT	10.950	0.01	CAS
57737.553	NOT	10.96	0.01	CAS
57741.072	TNO	10.95	0.01	CrAO, CAS
57742.091	TNO	10.90	0.10	Int
57743.237	TNO	10.83	0.10	Int
57746.144	TNO	10.74	0.01	CrAO, CAS
57747.137	TNO	10.71	0.01	CrAO, CAS
57752.570	CAHA	10.70	0.10	Int
57753.464	CAHA	10.69	0.10	Int
57754.497	CAHA	10.68	0.04	AAVSO
57757.407	NOT	10.63	0.01	CAS
57758.545	NOT	10.64	<0.01	AAVSO
57769.523	NOT	11.11	0.10	Int
57771.485	NOT	10.85	0.10	Int
57774.159	CrAO	10.99	0.01	CrAO
57776.205	CrAO	11.00	0.10	Int
57778.447	NOT	10.95	0.10	Int
57794.194	CrAO	10.93	0.01	CrAO
57797.186	CrAO	10.85	0.01	CrAO, CAS
57798.200	CrAO	10.87	0.10	Int
57799.180	CrAO	10.87	0.10	Int
57998.442	CrAO	10.82	0.01	CrAO
57999.442	CrAO	10.85	0.01	CrAO
58000.445	CrAO	10.72	0.01	CrAO
58025.441	CrAO	10.45	0.01	CrAO
58026.483	CrAO	10.42	0.10	Int
58027.476	CrAO	10.40	0.10	Int
58028.475	CrAO	10.38	0.10	Int
58029.435	CrAO	10.37	0.01	CAS
58030.438	CrAO	10.43	0.01	CAS
58031.438	CrAO	10.43	0.01	CAS
58082.248	CrAO	10.45	0.01	CrAO
58083.247	CrAO	10.51	0.01	CrAO
58085.234	CrAO	10.83	0.10	Int
58123.148	CrAO	10.46	0.01	CAS
58124.275	CrAO	10.37	0.10	Int
58125.149	CrAO	10.34	0.01	CrAO
58126.144	CrAO	10.41	0.01	CrAO, CAS
58145.229	CrAO	11.18	0.01	CrAO, CAS

Table A1 *– continued*

HJD 240 0000	Site	*V*	*V* error	Source of *V*
58183.200	CrAO	10.55	0.01	CrAO
58186.251	CrAO	–	–	–
58212.224	CrAO	10.54	0.01	CrAO
58213.225	CrAO	10.57	0.01	CrAO
58214.217	CrAO	10.65	0.10	Int
58215.220	CrAO	10.73	0.01	CrAO
58216.215	CrAO	10.77	0.01	CrAO
58217.219	CrAO	10.79	0.01	CrAO

Table A2. The *V* magnitudes of SU Aur for the dates of spectral observations. The Heliocentric Julian date (HJD) in the first column is followed by the site of the observation (CAHA, Calar Alto Observatory; CrAO, Crimean Astrophysical Observatory; NOT, Nordic Optical Telescope; TNO, Thai National Observatory; UrFU, Kourovka Astronomical Observatory), magnitude measured in the *V* band, corresponding error and source (CAS, Crimean Astronomical Station; AAVSO, American Association of Variable Star Observers; Int, value interpolated from AAVSO and CrAO photometry).

HJD 240 0000	Site	*V*	*V* error	Source of *V*
57288.462	CrAO	9.34	0.01	CrAO
57289.503	CrAO	9.39	0.01	CrAO
57290.490	CrAO	9.39	0.01	CrAO
57291.502	CrAO	9.33	0.01	CrAO
57301.500	CrAO	9.83	0.01	CrAO
57346.440	CrAO	9.50	0.01	CrAO
57347.510	CrAO	9.45	0.01	CrAO
57349.190	TNO	9.46	0.10	Int
57374.225	CrAO	9.43	0.01	CrAO
57378.333	CrAO	9.44	0.01	CrAO
57386.090	TNO	9.40	0.10	Int
57392.351	CrAO	9.41	0.10	Int
57395.086	TNO	9.50	0.01	AAVSO
57395.406	CAHA	9.50	0.01	AAVSO
57403.076	TNO	9.69	<0.01	AAVSO
57410.402	CAHA	9.72	0.01	AAVSO
57411.401	CAHA	9.61	0.10	Int
57414.412	CAHA	9.80	0.01	CrAO
57415.489	CAHA	9.73	0.10	Int
57426.373	CrAO	9.53	0.01	CrAO
57641.536	CrAO	9.42	0.01	CrAO
57642.517	CrAO	9.52	0.01	CrAO
57643.524	CrAO	9.43	0.01	CrAO
57644.467	CrAO	9.41	0.01	CrAO
57645.460	CrAO	9.39	0.01	CrAO
57646.481	CrAO	9.38	0.01	CrAO
57646.689	NOT	9.38	0.01	CrAO
57647.490	CrAO	9.52	0.01	CrAO
57679.623	NOT	9.42	<0.01	AAVSO
57681.613	NOT	9.51	0.01	AAVSO
57691.688	NOT	9.35	0.10	Int
57694.614	NOT	9.33	0.10	Int
57711.499	CrAO	9.30	0.01	CrAO
57712.584	CrAO	9.24	0.01	CrAO
57713.599	CrAO	9.28	0.01	CrAO
57714.486	CrAO	9.26	0.01	CrAO
57716.662	NOT	9.22	0.10	Int
57721.584	NOT	9.20	0.10	Int

Table A2 *– continued*

HJD 240 0000	Site	*V*	*V* error	Source of *V*
57728.213	CrAO	9.18	0.01	CrAO
57728.600	NOT	9.18	0.01	CrAO
57730.237	CrAO	9.20	0.01	CrAO
57730.465	NOT	9.20	0.01	CrAO
57732.643	NOT	9.19	0.10	Int
57735.584	CAHA	9.17	0.10	Int
57736.656	NOT	9.16	0.10	Int
57737.560	NOT	9.16	0.10	Int
57739.388	CrAO	9.15	0.01	CrAO
57741.072	TNO	9.19	0.01	CrAO
57742.091	TNO	9.20	0.10	Int
57743.237	TNO	9.21	0.10	Int
57746.144	TNO	9.21	0.01	CrAO
57747.135	TNO	9.18	0.01	CrAO
57752.617	CAHA	9.20	0.10	Int
57753.509	CAHA	9.21	0.10	Int
57754.547	CAHA	9.21	0.10	Int
57757.413	NOT	9.21	0.01	CrAO
57758.551	NOT	9.22	0.10	Int
57769.537	NOT	9.22	0.10	Int
57771.491	NOT	9.21	0.10	Int
57774.232	CrAO	9.21	0.01	CrAO
57776.273	CrAO	9.22	0.01	CrAO
57778.455	NOT	9.22	0.10	Int
57794.263	CrAO	9.32	0.01	CrAO
57797.259	CrAO	9.40	0.01	CrAO
57799.248	CrAO	9.44	0.10	Int
57998.513	CrAO	9.40	0.01	CrAO
57999.509	CrAO	9.30	0.01	CrAO
58000.510	CrAO	9.39	0.01	CrAO
58025.536	CrAO	9.41	0.01	CrAO
58026.549	CrAO	9.40	0.10	Int
58027.542	CrAO	9.40	0.10	Int
58028.540	CrAO	9.40	0.10	Int
58029.500	CrAO	9.40	0.10	Int
58030.503	CrAO	9.43	0.01	CAS
58031.502	CrAO	9.39	0.01	CAS
58049.473	UrFU	9.60	0.01	AAVSO
58082.322	CrAO	9.50	0.01	CrAO
58083.312	CrAO	9.46	0.01	CrAO
58085.302	CrAO	9.46	0.10	Int
58123.193	CrAO	9.74	0.01	CAS
58124.482	UrFU	9.98	0.01	AAVSO
58125.216	CrAO	10.01	0.01	CrAO
58125.404	UrFU	10.01	0.01	CAS
58126.210	CrAO	9.88	0.01	CrAO
58145.165	CrAO	10.76	0.01	CAS
58158.293	UrFU	9.60	0.01	AAVSO
58159.324	UrFU	9.66	0.01	AAVSO
58162.338	NOT	9.62	0.10	Int
58182.355	CrAO	9.45	0.01	CrAO
58183.266	CrAO	9.47	0.01	CrAO
58186.225	CrAO	9.62	0.10	Int
58212.262	CrAO	10.43	0.01	CrAO
58213.270	CrAO	10.74	0.01	CrAO
58214.242	CrAO	10.27	0.07	AAVSO
58215.265	CrAO	10.23	0.01	CrAO
58216.260	CrAO	10.01	0.01	CrAO

Table A3. RY Tau photometry. The values corresponding to the *UBVRI* photometry, taken between 1981 and 1997, are from the Majdanak archive (Grankin et al. 2007). All the *JHKLM* magnitudes were obtained at the Crimean Astronomical Station (CAS). The *BVRI* data corresponding to the period 2013–2018 were obtained at the CrAO.

HJD 240 0000	*U*	*B*	*V*	*R*	*I*	*J*	*H*	*K*	*L*	*M*
44888.400	–	–	–	–	–	7.80	6.65	5.55	–	–
44892.400	–	–	–	–	–	7.73	6.60	5.51	–	–
44902.600	–	–	–	–	–	7.78	–	5.61	–	–
46692.400	11.97	11.40	10.24	9.02	–	7.26	6.17	5.26	4.16	–
46694.386	11.90	11.29	10.15	8.95	–	7.34	6.19	5.25	4.08	3.74
47053.500	–	–	–	–	–	7.02	6.05	5.24	4.07	3.68
47126.500	–	–	–	–	–	7.26	6.24	5.35	–	3.65
47569.300	–	–	–	–	–	6.99	5.99	5.32	4.17	3.80
47825.369	11.81	11.20	10.09	8.96	–	7.15	6.12	5.26	4.09	3.70
50430.400	–	–	–	–	–	6.95	6.03	5.28	4.25	–
50484.300	–	–	–	–	–	6.88	5.92	5.39	4.21	3.82
57289.431	–	11.66	10.61	9.58	8.70	7.37	6.37	5.41	–	–
57291.500	–	11.84	10.78	9.72	8.80	7.47	6.40	5.44	4.23	3.88
57385.300	–	–	–	–	–	7.34	6.37	5.48	4.30	4.03
57391.291	–	11.77	10.73	9.66	8.76	7.36	6.39	5.47	4.31	4.09
57408.263	–	11.44	10.42	9.38	8.51	7.22	6.26	5.38	4.16	3.84
57427.300	–	11.93	11.01	10.06	9.16	7.52	6.39	5.41	4.14	3.89
57444.193	–	11.99	11.04	10.06	9.17	7.61	6.42	5.55	4.23	3.98
57453.200	–	11.89	11.00	10.04	9.20	7.60	6.45	5.41	4.16	3.91
57620.486	–	11.82	10.86	9.85	8.97	7.51	6.46	5.50	4.26	4.07
57623.500	–	11.84	10.87	9.85	8.95	7.51	6.45	5.46	4.20	4.11
57635.464	–	11.96	10.91	9.83	8.94	7.58	6.54	5.56	4.30	3.96
57638.500	–	–	–	–	–	7.61	6.52	5.53	4.25	3.92
57641.488	–	11.99	10.96	9.90	8.99	7.60	6.52	5.52	4.28	3.94
57648.492	–	11.91	10.95	9.93	9.09	7.68	6.59	5.57	4.27	3.92
57680.478	–	11.93	10.94	9.86	8.92	7.43	6.36	5.38	4.19	3.98
57704.400	–	12.08	11.21	10.15	9.27	7.68	6.55	5.50	4.19	4.03
57730.332	–	12.21	11.15	10.06	9.13	7.61	6.51	5.44	4.17	3.68
57745.300	–	11.80	10.68	9.50	8.57	7.30	6.28	5.39	4.11	3.80
57746.216	–	11.86	10.72	9.56	8.63	7.28	6.30	5.35	4.06	3.80
57767.208	–	12.21	11.12	9.97	9.02	7.54	6.43	5.44	4.15	3.98
57774.297	–	12.12	10.99	–	8.93	7.45	6.37	5.39	4.17	3.88
57777.200	–	–	–	–	–	7.53	6.42	5.41	4.15	4.01
57784.185	–	11.90	10.87	9.80	8.90	7.45	6.42	5.44	4.24	3.97
57785.272	–	11.95	10.85	–	–	7.41	6.38	5.44	4.20	4.02
57786.162	–	11.92	10.86	9.75	8.83	7.39	6.38	5.45	4.20	3.99
57795.200	–	11.93	10.90	9.80	8.85	7.33	6.31	5.37	4.13	3.88
57801.278	–	11.88	10.89	9.83	8.93	7.47	6.44	5.45	4.20	3.78
57803.189	–	11.86	10.88	9.88	9.05	7.56	6.48	5.51	4.20	3.88
57812.200	–	11.84	10.79	9.69	8.76	7.45	6.47	5.54	4.28	3.97
57813.226	–	11.84	10.78	9.68	8.76	7.39	6.38	5.52	4.21	3.94
57817.202	–	–	–	–	–	7.34	6.34	5.46	4.23	3.94
57998.512	–	11.85	10.81	9.67	8.76	7.42	6.42	5.49	4.31	3.95
58006.541	–	–	–	–	–	7.36	6.37	5.43	4.26	4.06
58026.513	–	–	–	–	–	7.20	6.28	5.42	4.20	3.88
58030.448	–	–	–	–	–	7.17	6.25	5.39	4.23	3.89
58038.489	–	–	–	–	–	7.24	6.32	5.43	4.27	3.97
58066.397	–	–	–	–	–	7.03	6.17	5.36	4.18	3.96
58096.465	–	11.43	10.40	9.29	8.44	7.22	6.32	5.44	4.20	3.95
58100.320	–	–	–	–	–	7.30	6.36	5.46	4.23	3.96
58114.436	–	11.78	10.73	9.65	8.75	7.29	6.34	5.38	4.10	3.62
58116.293	–	–	–	–	–	7.43	6.41	5.44	4.20	3.93
58120.251	–	–	–	–	–	7.23	6.25	5.36	4.19	3.90
58125.437	–	11.44	10.34	9.23	8.34	7.10	6.19	5.34	4.21	3.95
58126.210	–	11.54	10.41	9.29	8.39	7.14	6.23	5.36	4.19	3.91
58143.219	–	–	–	–	–	7.46	6.47	5.51	4.22	3.84
58145.209	–	–	–	–	–	7.46	6.45	5.48	4.28	4.03
58151.178	–	–	–	–	–	7.31	6.34	5.44	4.24	4.00

Table A4. SU Aur photometry. All the *JHKLM* magnitudes were obtained at the Crimean Astronomical Station (CAS). The *BVRI* data corresponding to the period 2013–2018 were obtained at the CrAO.

HJD 240 0000	*B*	*V*	*R*	*I*	*J*	*H*	*K*	*L*	*M*
57313.551	10.40	9.44	8.54	7.95	7.35	6.69	6.00	5.14	4.74
57324.290	10.77	9.75	8.79	8.11	7.47	6.77	6.02	5.06	4.80
57391.301	10.30	9.38	8.49	7.92	–	–	5.99	5.12	4.98
57399.372	10.27	9.34	8.44	7.91	7.36	6.67	6.03	5.12	4.99
57426.268	10.53	9.53	8.64	8.03	7.36	6.65	6.01	5.05	4.78
57623.524	10.16	9.33	8.42	7.86	7.27	6.57	5.94	5.05	5.16
57635.600	–	–	–	–	7.25	6.59	5.96	5.11	4.91
57638.500	–	–	–	–	7.32	6.66	6.02	5.13	4.86
57641.504	10.23	9.42	8.46	7.88	7.31	6.62	5.98	5.12	4.89
57648.474	10.35	9.48	8.51	7.95	7.37	6.69	6.02	5.12	4.92
57680.500	–	–	–	–	7.26	6.56	5.87	4.99	4.81
57704.600	10.10	9.23	8.38	7.83	7.22	6.54	5.92	5.08	4.99
57730.327	10.08	9.20	8.39	7.85	7.23	6.60	5.93	5.06	4.87
57745.456	10.08	9.24	8.40	7.84	7.30	6.72	6.08	5.23	5.03
57746.448	10.06	9.21	8.42	7.86	7.31	6.69	6.07	5.21	5.07
57774.399	10.02	9.21	8.36	7.82	7.26	6.67	6.05	5.18	4.98
57777.256	10.02	9.19	8.35	7.78	7.22	6.60	5.99	5.13	5.04
57785.257	10.04	9.22	8.37	7.83	7.28	6.66	6.04	5.20	5.10
57786.265	10.10	9.25	8.41	7.86	7.31	6.68	6.06	5.20	5.06
57795.232	10.17	9.33	8.44	7.89	7.38	6.72	6.02	5.19	5.00
57803.187	10.46	9.53	8.59	8.01	7.42	6.73	6.04	5.14	5.05
57812.300	–	–	–	–	7.44	6.76	6.07	5.14	5.06
57817.264	–	–	–	–	7.34	6.69	6.04	5.12	4.96
58004.501	10.16	9.30	8.43	7.90	7.25	6.62	5.96	5.09	4.95
58008.546	–	–	–	–	7.26	6.62	5.95	5.03	4.77
58026.556	–	–	–	–	7.23	6.58	5.92	5.00	4.78
58038.401	10.49	9.55	8.64	8.07	7.35	6.66	5.96	5.00	4.79
58066.348	10.55	9.61	8.66	8.10	7.34	6.64	5.90	4.91	4.69
58096.335	10.38	9.45	8.55	8.00	7.29	6.61	5.89	4.87	4.60
58100.369	–	–	–	–	7.35	6.66	5.91	4.92	4.64
58114.373	10.60	9.64	8.69	8.13	7.36	6.65	5.90	4.84	4.54
58120.191	10.66	9.67	8.71	8.12	7.31	6.63	5.87	4.87	4.63
58125.323	11.07	10.00	8.96	8.33	7.53	6.75	5.98	4.93	4.75
58126.193	10.94	9.88	8.88	8.25	7.46	6.73	5.96	4.91	4.67
58143.030	12.03	10.82	9.64	8.86	7.84	6.94	6.06	4.93	4.57
58144.238	11.95	10.72	9.56	8.79	7.81	6.94	6.03	4.94	4.64
58151.174	10.88	9.83	8.83	8.21	7.42	6.70	5.90	4.88	4.61

This paper has been typeset from a TEX/LATEX file prepared by the author.